1521-0103/359/3/392–400$25.00
THE JOURNAL OF PHARMACOLOGY AND EXPERIMENTAL THERAPEUTICS

http://dx.doi.org/10.1124/jpet.116.236562
J Pharmacol Exp Ther 359:392–400, December 2016

Akebia Saponin D Decreases Hepatic Steatosis through Autophagy Modulation[S]

Li-li Gong, Guang-run Li, Wen Zhang, He Liu, Ya-li Lv, Fei-fei Han, Zi-rui Wan, Ming-biao Shi, and Li-hong Liu

Beijing Chao-Yang Hospital, Capital Medical University, Beijing, China

Received July 12, 2016; accepted September 20, 2016

ABSTRACT

Nonalcoholic fatty liver disease (NAFLD) is considered to be a hepatic manifestation of the metabolic syndrome, and the incidence of NAFLD is increasing rapidly. However, appropriate drugs for treatment of NAFLD are lacking. This study aimed to elucidate the protective effects and mechanisms of Akebia saponin D (ASD) against NAFLD in ob/ob mice and Buffalo rat liver cells. ASD significantly decreased hepatic steatosis and hepatocyte apoptosis in ob/ob mice. ASD also significantly activated autophagic flux, as assessed by the decreased expression of light chain 3 (LC3)-II and P62 accumulation of autophagosomes. In Buffalo rat liver cells, ASD prevented oleic acid (OA)–induced lipid droplets and increased autophagic flux acting as increase the number of autolysosomes than autophagosomes in mTagRFP-mWasabi-LC3. ASD treatment also prevented OA-induced expression of LC3-II, P62, Beclin, and phospho–mammalian target of rapamycin. These effects were similar to those of cotreatment with rapamycin. ASD treatment could not prevent OA-increased, autophagy-related protein expression after treatment with chloroquine or small interfering RNA–mediated knockdown of atg7. These results suggest that ASD alleviates hepatic steatosis targeted at the fusion of autophagosomes to lysosomes, and autophagy modulation via ASD may offer a new strategy for treating NAFLD.

Introduction

Nonalcoholic fatty liver disease (NAFLD) represents a spectrum of liver disease ranging from pure fatty liver and nonalcoholic steatohepatitis to fibrosis and irreversible cirrhosis that occurs in patients who do not consume significant amounts of alcohol (Matteoni et al., 1999). NAFLD is strongly associated with components of the metabolic syndrome, including obesity, hypertension, dyslipidemia, and insulin resistance; in fact, NAFLD is now recognized to represent the hepatic manifestation of the metabolic syndrome (Smith and Adams, 2011). NAFLD occurs in developed and developing countries, making it the most common liver condition in the world (Lazo and Clark, 2008). Although a large number of studies have been conducted, the pathophysiology of NAFLD is complicated and not completely elucidated.

NAFLD has been linked to lipid accumulation and lipid metabolism dysfunction. Recent studies have shown that autophagy is involved in lipid metabolism. Hepatic autophagy degraded lipid droplets to provide free fatty acids (FFAs) for ATP production when increase lipid availability. In contrast, hepatic autophagy turnover was inhibited if lipids were sustained by a long-lasting, high-fat diet (HFD). Singh et al. (2009) reported that lipid metabolism was regulated by autophagy through eliminating triglycerides (TGs) and preventing the development of steatosis. Decreased autophagic function may promote the initial development of hepatic steatosis (Czaja, 2010). Prior studies demonstrated that genetic leptin-deficient ob/ob mice, which show obesity and insulin resistance, develop NAFLD similar to that observed in humans, and these mice are commonly used as an animal model of NAFLD. Investigators observed defective autophagy in studies in ob/ob mice (Yang et al., 2010). Autophagy markers, as indicated by light chain 3 (LC3)-II accumulation and P62 degradation, were impaired in the liver of ob/ob mice. Consistently, autophagy-associated proteins such as Autophagy-related protein 7 (Atg7), Beclin-1, and Autophagy protein 5 (Atg5)–Autophagy-related protein 12 (Atg12) conjugation were downregulated. Therefore, activation of autophagy in hepatocytes could constitute a therapeutic approach against hepatic complications.

Akebia saponin D (ASD; also named Asperosaponin VI) (Supplemental Fig. 1) is a typical bioactive triterpenoid saponin isolated from the rhizome of *Dipsacus asper Wall*, which has long been used as an antiosteoporosis drug (Yu et al., 2012).

This research was supported by the National Natural Science Foundation of China [Grant 81302822], the Beijing Municipal Administration of Hospitals' Youth Programme [Grant QML20150302], and the Capital Medical University [Grant 15ZY02].
dx.doi.org/10.1124/jpet.116.236562.
[S] This article has supplemental material available at jpet.aspetjournals.org.

ABBREVIATIONS: ALT, alanine transaminase; ASD, Akebia saponin D; AST, aspartate transaminase; BRL, Buffalo rat liver; BSA, bovine serum albumin; CQ, chloroquine; DMEM, Dulbecco's modified Eagle's medium; EGFP, enhanced green fluorescent protein; FBS, fetal bovine serum; FFA, free fatty acid; GSH-PX, glutathione peroxidase; HFD, high-fat diet; HOMA-IR, homeostasis model assessment of insulin resistance; MDA, malondialdehyde; mTOR, mammalian target of rapamycin; NAFLD, nonalcoholic fatty liver disease; OA, oleic acid; PCR, polymerase chain reaction; PVDF, polyvinylidene difluoride; RFP, red fluorescent protein; siRNA, small interfering RNA; SM, silibinin meglumine; SOD, superoxide dismutase; TC, total cholesterol; TG, triglyceride; TUNEL, terminal deoxynucleotidyl transferase–mediated digoxigenin-deoxyuridine nick-end labeling.

ASD is demonstrated to have some therapeutic effects on some disease models, such as cancer (Jeong et al., 2008), Alzheimer disease (Jeong et al., 2008; Zhou et al., 2009; Yu et al., 2012), cardiovascular disease (Li et al., 2010a,b, 2012), and bone fractures (Peng et al., 2010; Niu et al., 2011). We previously showed that ASD exerts hepatoprotective effects on acute liver injury induced by carbon tetrachloride in mice (Li et al., 2012) and against rotenone-induced toxicity in Buffalo rat liver (BRL) cells (Gong et al., 2014). These findings suggest that ASD has a hepatoprotective effect. However, the beneficial effects of ASD on NAFLD have not been fully investigated. Therefore, in this study, we investigated the protective effect of ASD against NAFLD in leptin-deficient ob/ob mice and BRL cells.

Materials and Methods

Drugs, Reagents, and Plasmids

ASD was extracted at Beijing Chao-Yang Hospital (affiliated with Beijing Capital Medical University, Beijing, China) and its structure was confirmed on the basis of physicochemical properties and spectral evidence (Lan et al., 2011). ASD standard (92.5% purity, batch no. 11685-200802) was purchased from the National Institutes for Food and Drug Control (Beijing, China). ASD purity was calculated based on the following external standard method:

$$\text{Purity } (\%) = \frac{\frac{C_{Standard}}{A_{Standard}} \times A_{Sample} \times V_{Sample}}{M_{Sample}} \times 100\%$$

where C is the concentration, A is the peak area, and M is the sample weight. ASD purity was more than 98%, as tested by a high-performance liquid chromatography method (Supplemental Fig. 2).

Silibinin meglumine (SM) was a generous gift from Shanghai Seebio Biotech (Shanghai, China). Fetal bovine serum (FBS) and Dulbecco's modified Eagle's medium (DMEM) were obtained from HyClone Laboratories (Logan, UT). Oleic acid (OA), rapamycin, chloroquine (CQ), and bovine serum albumin (BSA) were from Sigma-Aldrich (St. Louis, MO). Immobilon polyvinylidene difluoride (PVDF) membrane was purchased from Millipore (Billerica, MA).

Aspartate transaminase (AST) and alanine transaminase (ALT) diagnostic biochemical assay kits were obtained from Biosino Biotechnology Company Ltd. (Beijing, China). TG, total cholesterol (TC), FFAs, fasting glucose, fasting insulin, superoxide dismutase (SOD), glutathione peroxidase (GSH-PX), and malondialdehyde (MDA) diagnostic agents were obtained from Nanjing Jiancheng Bioengineering Institute (Nanjing, China).

EGFP-LC3, mTagRFP-mWasabi-LC3, and mTagRFP-mWasabi-LC3ΔG plasmids were a generous gift from Dr. Jian Lin (Peking University, Beijing, China). Microtubule-associated protein LC3 is a ubiquitin-like protein that binds to autophagosomes, and enhanced green fluorescent protein (EGFP)–tagged LC3 was subsequently used to track and follow the fate of autophagosomes in the cell. The mTagRFP-mWasabi-LC3 plasmid consists of a red fluorescent protein (RFP) (mTagRFP), a green fluorescent protein (mWasabi), and an amino terminal of the autophagy-labeled protein (LC3), which was used to monitor autophagic flux. In green/red merged images, yellow puncta (i.e., RFP-positive, Wasabi-positive) indicate autophagosomes, whereas red puncta (i.e., RFP-positive, Wasabi-negative) indicate autolysosomes. mTagRFP-mWasabi-LC3ΔG was constructed as the negative control.

Studies in ob/ob Mice

Animals. Six-week-old male C57BL/6 and leptin-deficient ob/ob mice were purchased from the Fourth Military Medical University Experimental Animal Center (Xi'an, China) [license no. SCXK (JUN) 2007-007]. The mice were housed individually under conditions controlled for temperature (24°C ± 5°C), humidity (55% ± 5%), and light (12-hour/12-hour light/dark cycle). After acclimating for 1 week, nine C57BL/6 male mice that were fed a standard purified rodent diet served as controls. The ob/ob mice were fed a HFD and randomly divided into five groups. The mice were administered vehicle (saline), ASD (30, 60, and 120 mg/kg per day), or SM (20 mg/kg per day) via intraperitoneal injection for 4 weeks. All experiments were carried out in accordance with China animal welfare legislation and were approved by the Beijing Chao-Yang Hospital Committee on Ethics in the Care and Use of Laboratory Animals.

At the end of the experiment, mice were anesthetized with urethane (1 g/kg, i.p.) and body weights, liver weights, and fat pad weights were measured. Blood samples were collected from the inner canthus, and livers were removed immediately and washed in prechilled physiologic saline. A SpectraMax M5 microplate reader (Molecular Devices, Sunnyvale, CA) was used, according to the manufacturer's instructions, to measure the following: levels of AST, ALT, fasting glucose, and fasting insulin in the blood; activity of SOD, MDA, and GSH-PX; and levels of TG, TC, and FFA in liver tissues. Values for the homeostasis model assessment of insulin resistance (HOMA-IR) were estimated by dividing the product of fasting glucose (in millimoles) and insulin levels (in milli-international units per liter) by 22.5.

Hematoxylin and Eosin Staining. The livers were washed immediately with saline and then fixed in 4% buffered paraformaldehyde solution. Paraffin-embedded liver biopsy sections (5 μm) were stained with hematoxylin and eosin for histologic analysis. These sections were examined under a light microscope for histoarchitectural changes, and photomicrographs were then taken. Image-Pro Plus 6.0 software (Media Cybernetics, Rockville, MD) was used to evaluate the degree of hepatocellular ballooning and lobular inflammation (grade of activity).

TUNEL Assay. A terminal deoxynucleotidyl transferase–mediated digoxigenin-deoxyuridine nick-end labeling (TUNEL) assay was performed using the POD In Situ Cell Death Detection kit according to the manufacturer's instructions (Roche Diagnostics, Indianapolis, IN). For each liver, the total number of TUNEL-positive hepatocyte nuclei was counted in 10 sections. Individual nuclei were visualized at ×200 magnification, and the percentage of apoptotic nuclei (apoptotic nuclei/total nuclei) was calculated in six randomly chosen fields per slide and averaged for statistical analysis.

Electron Microscopy Ultrastructural Examination. Small pieces of liver were taken and rinsed in 0.1 M phosphate buffer solution (PBS, pH 7.2). Liver pieces of approximately 1 mm^3 were trimmed and immediately fixed in ice-cold glutaraldehyde (3%) plus *p*-formaldehyde (4%) in 0.1 M phosphate buffer and kept at 4°C for 2 hours. Samples were postfixed in 1% osmium tetroxide for 60 minutes at 25°C. After dehydration in a graded series of ethanol, liver pieces were embedded in spur resin. Thin sections (60 nm) were cut on an Ultramicrotome (Leica Microsystems, Buffalo Grove, IL). The sectioned grids were stained with saturated solutions of uranyl acetate and lead citrate. The sections were examined using an electron microscope (H-7650; Hitachi, Tokyo, Japan).

Immunohistochemistry. The slides were stained with primary anti-LC3 antibody (Cell Signaling Technology, Danvers, MA). An anti–rabbit horseradish peroxidase/3,3′-diaminobenzidine detection system was used to visualize the expression according to the manufacturer's protocol. Positive and negative controls were established to identify any nonspecific staining. For negative controls, the primary antibody was replaced with normal rabbit IgG (Vector Laboratories, Burlingame, CA). All slides were viewed using an Olympus microscope (Tokyo, Japan).

Western Blot Analysis for Autophagy. Liver tissue lysates were subjected to SDS-PAGE and electrophoretically transferred to a PVDF membrane. The membranes were then exposed to primary antibodies (LC3, P62, and Beclin1; Cell Signaling Technology) overnight at 4°C. After incubation with the IRDye 680LT secondary antibody (LI-COR Biosciences, Lincoln, NE) for 1 hour at room temperature, immunoreactive proteins were visualized by using an Odyssey Infrared Imaging System (LI-COR Biosciences).

Studies in BRL Cells

Cell Culture and Treatment. BRL cells have been widely used for liver biologic and chemical studies. BRL cells were purchased from the Cell Center of Shanghai Institutes for Biologic Sciences (Shanghai, China). Cells were cultured in DMEM supplemented with 10% (v/v) FBS at 37°C with 5% CO_2. OA (20 mM) in 0.01 N NaOH was incubated at 70°C for 30 minutes and then mixed with 10% BSA in PBS at a 1:9 molar ratio of OA/BSA. The OA-BSA conjugate was administered to the cultured cells. BSA was used as a vehicle control. BRL cells were pretreated with various concentrations of ASD (1, 10, and 100 μM) for 1 hour, followed by incubation with 200 μM OA or vehicle control for 24 hours. Rapamycin (25 ng/ml) and CQ (50 nM) were used as negative and positive controls of autophagosome accumulation.

Lipid Droplet Staining. BRL cells were fixed in 4% paraformaldehyde in PBS for 30 minutes, washed thoroughly with PBS, and incubated with the specific Bodipy 493/503 neutral lipid probe (10 μg/ml; Invitrogen, Carlsbad, CA) at room temperature for 1 hour in the dark. The cells were visualized under fluorescence microscopy.

Cell Culture and Transfection. BRL cells were cultured in DMEM (HyClone Laboratories) supplemented with 10% FBS at 37°C in a 5% CO_2 atmosphere. Approximately 1×10^6 cells were plated in a confocal dish 24 hours before transfection. The EGFP-LC3 plasmid was usually used to detect autophagy. The mTagRFP-mWasabi-LC3 reporter is sensitive and accurate in detecting the accumulation of autophagosomes and autolysosomes and is used for monitoring autophagic flux. Meanwhile, mTagRFP-mWasabi-LC3ΔG was used as the negative control. Plasmid transfections (800 ng/well for EGFP-LC3, mTagRFP-mWasabi-LC3, and mTagRFP-mWasabi-LC3ΔG) were performed with Lipofectamine 2000 (Invitrogen) according to the manufacturer's protocol (Zhou et al., 2012). The cells were observed with confocal microscopy without fixation.

RNA Interference. BRL cells were transfected with small interfering RNAs (siRNAs) targeting atg7 (GenePharma, Suzhou, China) or with a control siRNA (GenePharma) using Lipofectamine 2000 (Invitrogen) according to the manufacturer's instructions. Cells were incubated for 16 hours with a transfection mixture containing a final siRNA concentration of 100 pM and were then supplemented with fresh medium. RNA was extracted from cell culture lysates using TRIzol reagent (Invitrogen) according to standard protocol.

Real-Time Polymerase Chain Reaction Analysis. Real-time polymerase chain reaction (PCR) analysis was used to quantify differences in gene expression. Target gene expression was normalized to that of an internal reference (glyceraldehyde-3-phosphate dehydrogenase). Real-time PCR was performed with primers and SYBR Premix Ex Taq (Takara, Shiga, Japan) in a Cobas z 480 real-time PCR machine (Roche Diagnostics). Target sequences were amplified using the following thermal conditions: 2 minutes at 95°C, and 45 cycles of 10 seconds at 95°C and 30 seconds at 68°C. All reactions were performed in triplicate. Expression levels of the genes of interest were presented as the relative levels to the mRNA level of the control gene.

Western Blot Analysis. Cells were harvested and lysed in protein lysis buffer (Applygen, Beijing, China). Proteins were separated in SDS-PAGE and transferred to PVDF membranes. Membranes were incubated overnight at 4°C with the primary antibodies (Atg7, LC3; Cell Signaling Technology). The membranes were washed and then incubated with IRDye 680LT secondary antibody (LI-COR Biosciences) for 1 hour at room temperature on an orbital shaker. After washing, bands were detected using the Odyssey Infrared Imaging System.

Statistical Analysis

Results are expressed as means ± S.E.M. in each group. To examine differences between groups, initial analyses were conducted with one-way analysis of variance followed by the Dunnett test. If the data did not fit the constraints of the parametric test, the data were analyzed with the chi-square test, Kruskal–Wallis analysis of variance, or Mann–Whitney test. A P value < 0.05 was considered statistically significant.

Results

ASD Treatment Decreased Plasma Lipids and Hepatic Steatosis in ob/ob Mice. Body weights, liver weights, and fat pad weights were calculated at the end of the experiments. We found that HFD ob/ob mice had higher body weights, liver weights, and fat pad weights compared with C57BL/6J mice. ASD treatment significantly inhibited the HFD-induced indices of adiposity and liver/body weight in ob/ob mice.

The effects of ASD on glycemic control and insulin resistance are shown in Supplemental Table 1. Serum glucose levels were significantly lower in ASD-treated mice than in ob/ob mice ($P < 0.05$). Serum insulin levels were significantly increased in the ob/ob group compared with the control group. Compared with ob/ob mice, ASD-treated mice had significantly reduced levels of both these parameters ($P < 0.05$) and HOMA-IR values ($P < 0.01$).

There was a marked accumulation of fat droplets in the livers of ob/ob mice, and ballooning degeneration was also seen (Fig. 1B). ASD-treated obese mice displayed decreased hepatic steatosis (Fig. 1, D–F). The livers of SM-treated animals showed mild to moderate fat droplets (Fig. 1C). Likewise, the hepatic TG concentration decreased from 71.2 ± 3.5 mg/g in untreated obese mice to 38.6 ± 1.8, 22.7 ± 4.6, and 14.3 ± 5.6 mg/g liver in ASD-treated animals ($P < 0.001$ versus ob/ob mice) (Fig. 1G). In these mice, however, hepatic TG content was significantly higher than in wild-type mice (7.97 ± 5.2 mg/g wet liver; $P < 0.001$). Levels of hepatic TC and FFAs in the ASD-treated group were reduced compared with the ob/ob group ($P < 0.05$; Fig. 1, H and I).

ASD Treatment Protected against NAFLD-Induced Liver Damage. To test whether ASD could protect against NAFLD liver apoptosis, we performed TUNEL assays and ultrastructural examinations and assessed hepatic AST, ALT, SOD, GSH-PX, and MDA. The frequency of TUNEL-positive cells expressed as a percentage of the total nuclei was significantly increased in ob/ob mice (82.35% ± 2.14%). Liver tissues demonstrated a marked appearance of dark brown apoptotic cells (Fig. 2Ab). In contrast, almost no apoptotic cells were observed in normal control C57BL/6J mice (Fig. 2Aa). The number of TUNEL-positive cells significantly decreased after ASD treatment (40.28% ± 1.37% 33.25% ± 1.20%, and 22.39% ± 2.16% for 30 mg/kg, 60 mg/kg, and 120 mg/kg, respectively) (Fig. 2Cf).

Figure 2B presents results of transmission electron microscopy studies of hepatocyte nucleoli in the experimental group. In contrast with normal liver tissue (Fig. 2Ba), we found shrunken hepatocytes and broken nucleoli (Fig. 2Bb). Electron micrographs of the nucleoli of ASD-treated (30, 60, and 120 mg/kg) mice showed less apoptosis in a dose-dependent manner. Nucleoli in the liver tissue of ASD-treated (120 mg/kg) mice displayed near normal architecture.

Compared with C57BL/6 mice, activity of the serum hepatic injury marker enzymes AST (248.26 ± 12.55 U/L) and ALT (346.18 ± 20.35 U/L) was significantly increased in ob/ob mice. Treatment with 30 mg/kg, 60 mg/kg, and 120 mg/kg ASD, respectively, restored almost all alterations of AST (162.46 ± 11.59 U/L, 145.69 ± 12.70 U/L, and 121.40 ± 18.21 U/L) and ALT (212.08 ± 20.62 U/L, 176.24 ± 19.97 U/L, 126.52 ± 16.89 U/L) to near normal levels.

We observed a significant increase in MDA content as well as significant declines in SOD and GSH-PX activity in the liver tissues of ob/ob mice. Administration of ASD (30, 60, and

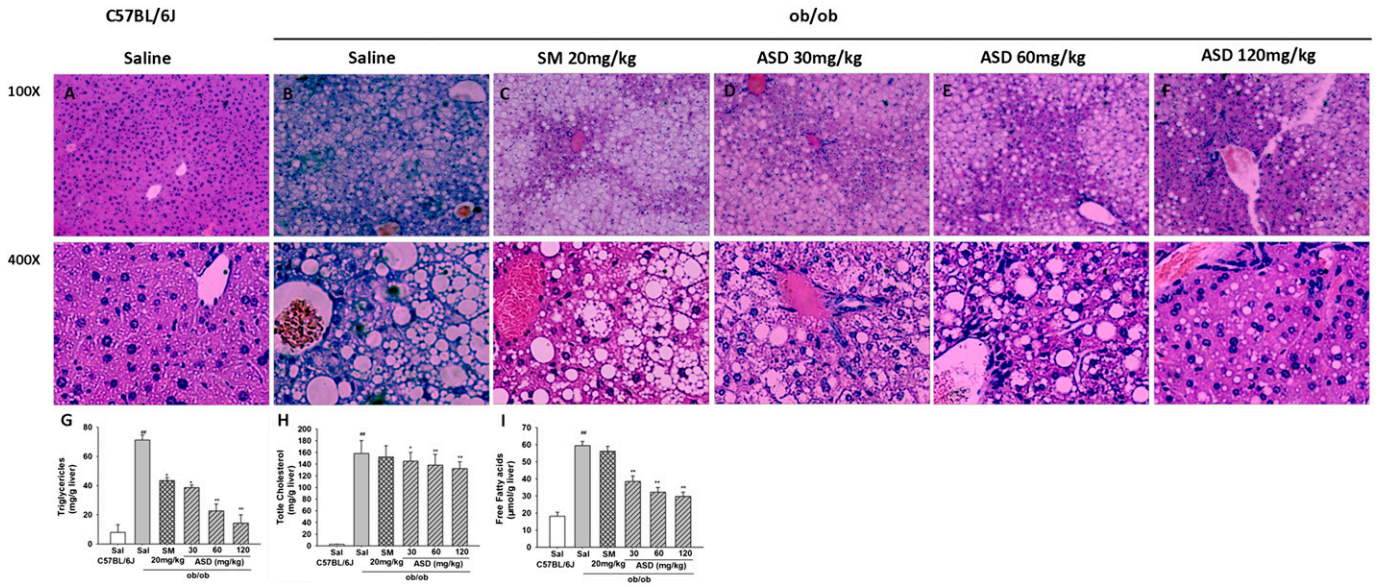

Fig. 1. Effects of ASD on liver morphology in ob/ob mice. (A) C57BL/6 mice showed normal hepatocytes with a distinctive membrane, abundant cytoplasm, and regular oval nuclei. (B) ob/ob mice treated with saline intraperitoneally for 4 weeks showed a marked accumulation of fat droplets. (C) ob/ob mice treated with SM (20 mg/kg per day) for 4 weeks showed mild to moderate fat droplets. (D–F) ob/ob mice treated with 30 mg/kg per day ASD (30, 60, and 120 mg/kg per day, i.p., respectively) for the same time period. ASD-treated obese mice displayed decreased hepatic steatosis. Hematoxylin and eosin staining results are shown in (A) through (F). (G–I) Concentration of liver TG, TC, and FFAs. ASD-treated mice had significantly decreased hepatic TG, TC, and FFA levels. Results are presented as means ± S.E.M. ($n = 6$). *$P < 0.05$ (compared with ob/ob mice); **$P < 0.01$ (compared with ob/ob mice); $^{\#\#}P < 0.01$ (compared with normal control). Sal, saline. Original magnification, ×100 in (A–F, top) and ×400 in (A–F, bottom). Scale bar, 400 μm in (A–F, top) and 200 μm in (A–F, bottom).

120 mg/kg) markedly attenuated alterations in antioxidant enzymes (Fig. 2, Ca–Ce).

ASD Treatment Activated Autophagy in Liver Tissue. We performed electron microscopy to analyze autophagosome formation. Autophagosome levels significantly increased in the liver of ASD-treated (30, 60, and 120 mg/kg) mice (Fig. 3A). Liver samples were also used to determine the immunohistological staining for LC3-II. Liver tissues taken from normal control C57BL/6J mice demonstrated little stain for LC3-II (Fig. 3Ba); ob/ob mice had an increased degree of positive staining for LC3-II (Fig. 3Bb), although LC3-II staining was significantly reduced in ASD-treated (30, 60,

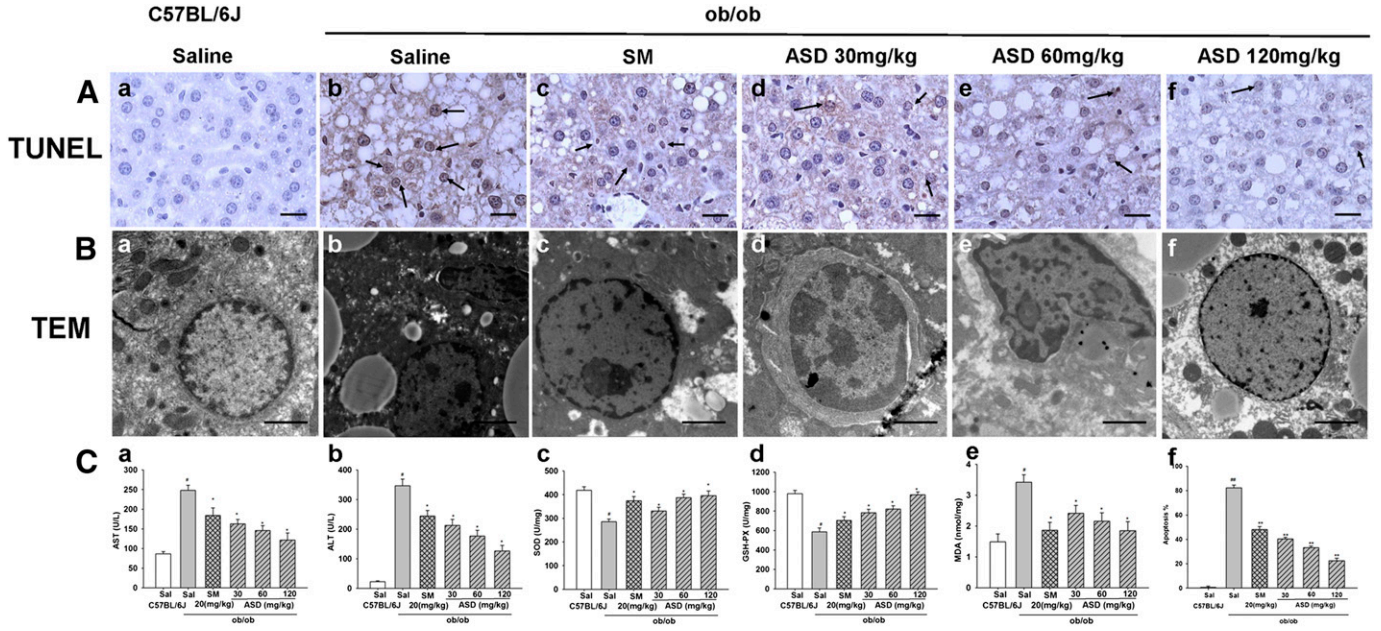

Fig. 2. Effect of ASD on hepatocyte apoptosis in ob/ob mice. (Aa and Ba) Normal group with no apoptotic cells. (Ab and Bb) ob/ob mice treated with saline intraperitoneally for 4 weeks showed significantly more TUNEL-positive apoptotic cells. Transmission electron microscopy results showed shrunken hepatocytes and broken nucleoli (Bb) and the increase in apoptotic cells was significantly attenuated by ASD treatment (30, 60, and 120 mg/kg per day, respectively) (Bd–Bf). (Ac and Bc) SM (20 mg/kg per day) also decreased apoptotic cells. (Ca and Cb) Effect of ASD on AST and ALT serum marker enzymes in ob/ob mice. (Cc–Ce) Effect of ASD on liver levels of SOD, MDA, and GSH-PX in ob/ob mice. (Cf) Effects of ASD on the number of TUNEL-positive cells. Results are presented as means ± S.E.M. ($n = 6$). *$P < 0.05$ (compared with ob/ob mice), $^{\#}P < 0.05$ (compared with normal control); **$P <$ 0.01 (compared with ob/ob mice); $^{\#\#}P < 0.01$ (compared with normal control). Sal, saline. Scale bar, 100 μm in (A) and 50 μm in (B).

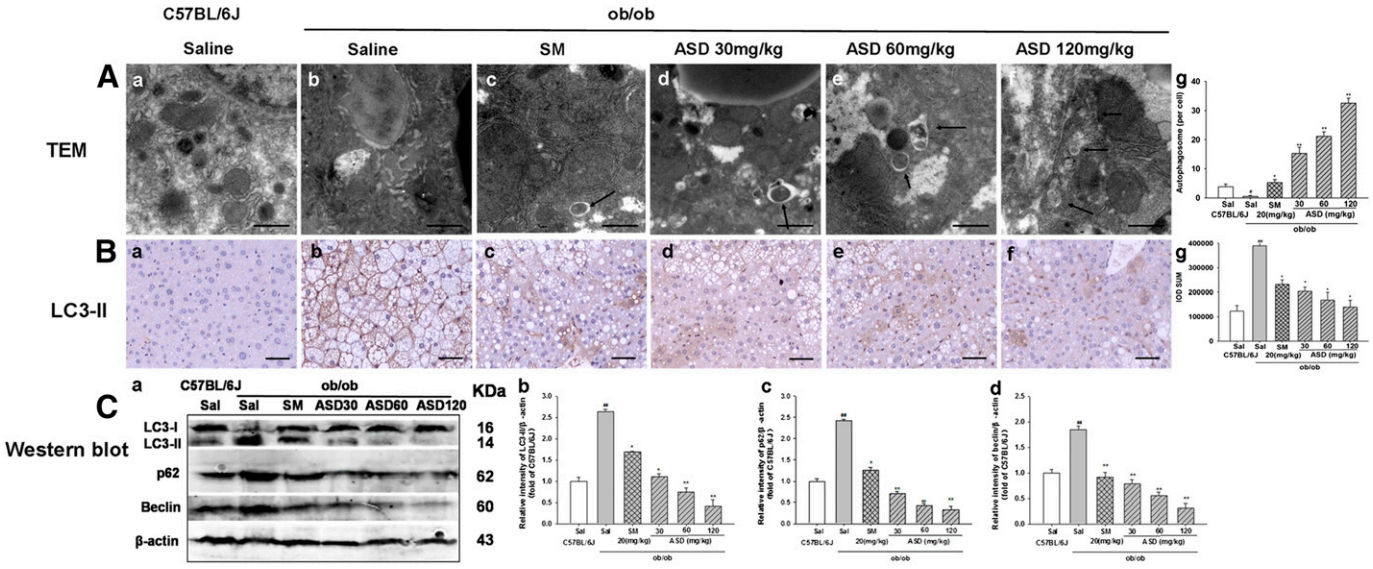

Fig. 3. Effects of ASD on autophagy in livers of ob/ob mice. (A) Electron microscopy shows the ultrastructure of mice livers. Arrows indicate autophagosomes. (B) Immunohistochemistry for LC3-II. (C) Western blot analysis of the levels of LC3-II, P62, and Beclin. All values are means ± S.E.M. ($n = 6$). $^{*}P < 0.05$ (compared with ob/ob mice); $^{**}P < 0.01$ (compared with ob/ob mice); $^{\#\#}P < 0.01$ (compared with normal control). Scale bar, 20 μm in (A) and 100 μm in (B) a-normal group, b-ob/ob mice group, c-SM group, d-ASD 30 mg/kg, e-ASD 60 mg/kg, f-ASD 120 mg/kg.

and 120 mg/kg) ob/ob mice (Fig. 3, Bd–Bg). In addition, we also measured the levels of proteins that are specifically involved in autophagy. LC3-II, P62, and Beclin levels were significantly increased in ob/ob mice livers (Fig. 3C). On the contrary, ASD treatment (30, 60, and 120 mg/kg) decreased LC3-II, P62, and Beclin expression.

ASD Reduced Hepatocyte Lipid Accumulation in BRL Cells. To further confirm the role of ASD in the reduction of hepatocyte lipid accumulation, we performed studies on BRL cells. As shown in Fig. 4, BRL cells were fixed and stained with Bodipy 493/503, a fluorescent dye that specifically stains intracellular lipid droplets. OA treatment significantly increased the number of lipid droplets in BRL cells. In contrast, lipid droplets were barely detectable in the BSA-treated control, and very limited lipid staining was observed in the BRL cells treated with ASD (1, 10, and 100 μM).

ASD Increased Autophagic Flux. We then determined the effects of ASD on OA-induced EGFP-LC3 puncta. We found that ASD (1, 10, and 100 μM) significantly enhanced OA-induced EGFP-LC3 puncta formation (Fig. 5A). In addition to monitoring autophagosomes, assays for monitoring

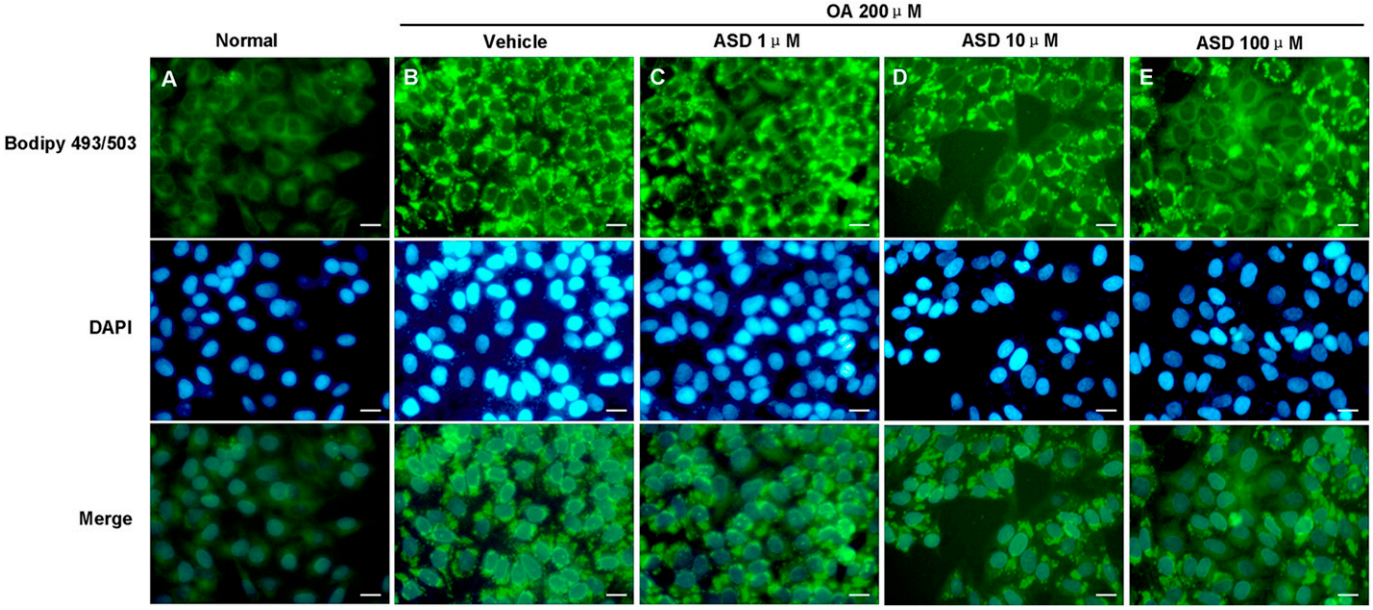

Fig. 4. ASD reduces OA-induced lipid accumulation in BRL cells. (A) Normal control showed no lipid accumulation. (B) Treatment with OA (200 μM) significantly increased intracellular lipid accumulation. (C–E) In contrast, pretreatment with ASD (1, 10, and 100 μM) for 1 hour before OA exposure significantly reduced OA-induced lipid accumulation, as assessed by visualization of Bodipy 493/503 staining. DAPI, 4',6-diamidino-2-phenylindole. Scale bar, 100 μm.

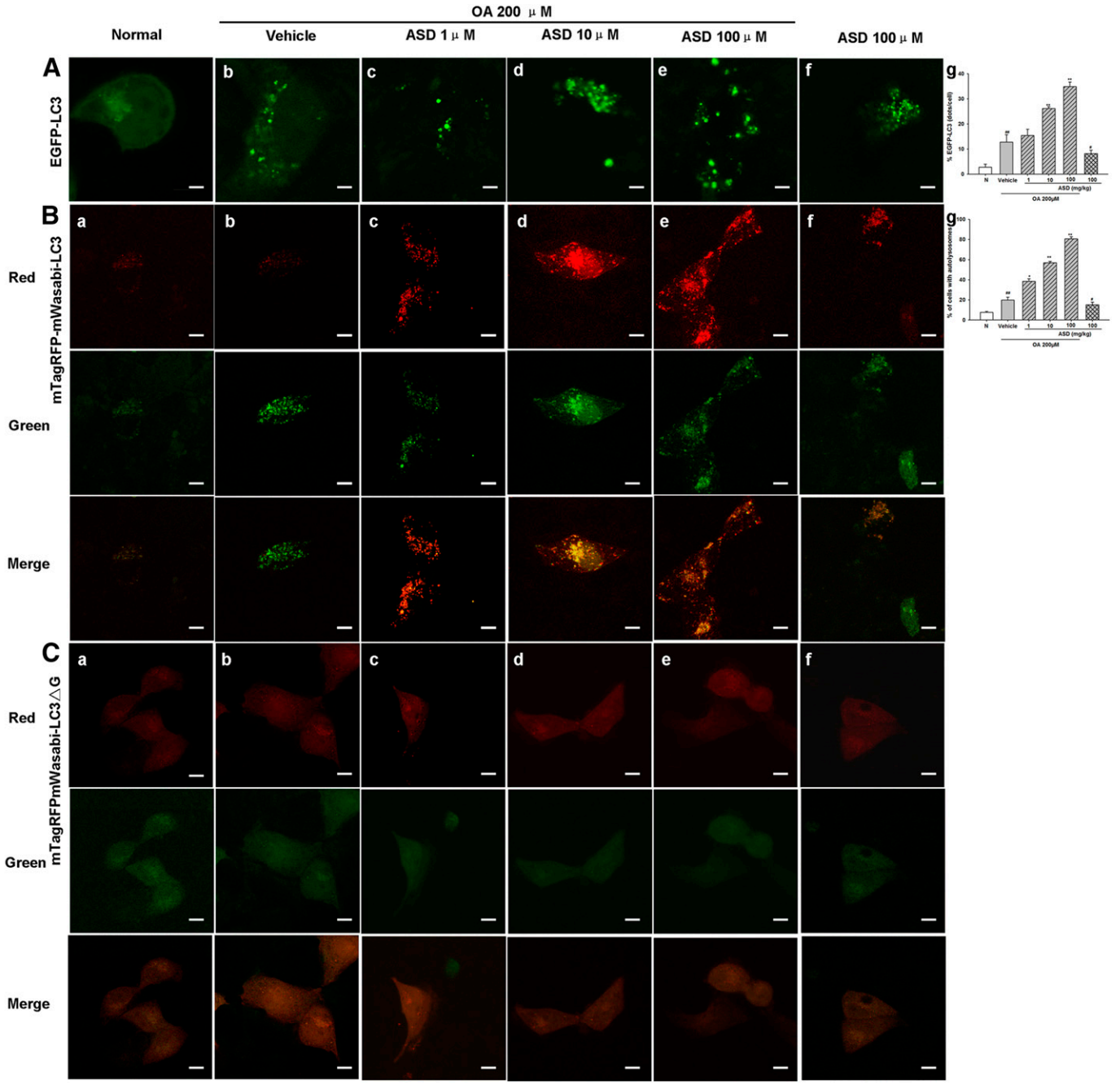

Fig. 5. ASD increases autophagic flux. Representative fluorescent images of BRL cells transiently transfected with EGFP-LC3. (A–C) Quantitation of autophagic cells based on the percentage of EGFP-LC3–positive cells with EGFP-LC3 dots (A), mTagRFP-mWasabi-LC3 (B), and mTagRFP-mWasabi-LC3ΔG (C). Comparison of both green and red fluorescent signals of mTagRFP-mWasabi-LC3 in different conditions. Cells with autolysosomes and/or autolysosomes were samples from a pool of at least 10 images. Scale bar, 50 μm a-normal group, b-OA 200 μM group, c-OA 200 μM+ ASD1 μM group, d-OA 200 μM+ASD 10 μM, e-OA 200 μM+ASD 100 μM, f-ASD 100 μM.

autophagic flux were also developed and mTagRFP-mWasabi-LC3 plasmid was used. In green/red merged images, yellow puncta indicate autophagosomes, whereas red puncta indicate autolysosomes. In ASD-treated (1, 10, and 100 μM) BRL cells, ASD induced more autolysosomes than autophagosomes, indicating that autophagic flux is increased in cells (Fig. 5B).

Molecular Evidence for Autophagy Induction by ASD. We next measured the expression of autophagy-related proteins LC3-II, P62, Beclin, and mTOR in BRL cells. OA treatment of BRL cells resulted in an increase in LC3-II (Fig. 6Aa). We also found that accumulation of P62 was parallel to an increase in LC3-II, reflecting a loss of autophagic flux (Fig. 6Aa). In addition, Beclin expression levels and mTOR phosphorylation levels were also increased after OA treatment. ASD treatment (100 μM) prevented OA-induced expression of LC3-II, P62, Beclin, and phospho-mTOR. Under the same experimental conditions, rapamycin decreased P62 and the LC3-II/LC3-I ratio in OA-treated cells compared with cells treated with OA alone, indicating a recovery of autophagic flux (Fig. 6Ab). ASD treatment (100 μM) exhibited almost the same effect as rapamycin (Fig. 6Ab) but could not attenuate the autophagic flux blocked by CQ (Fig. 6Ac).

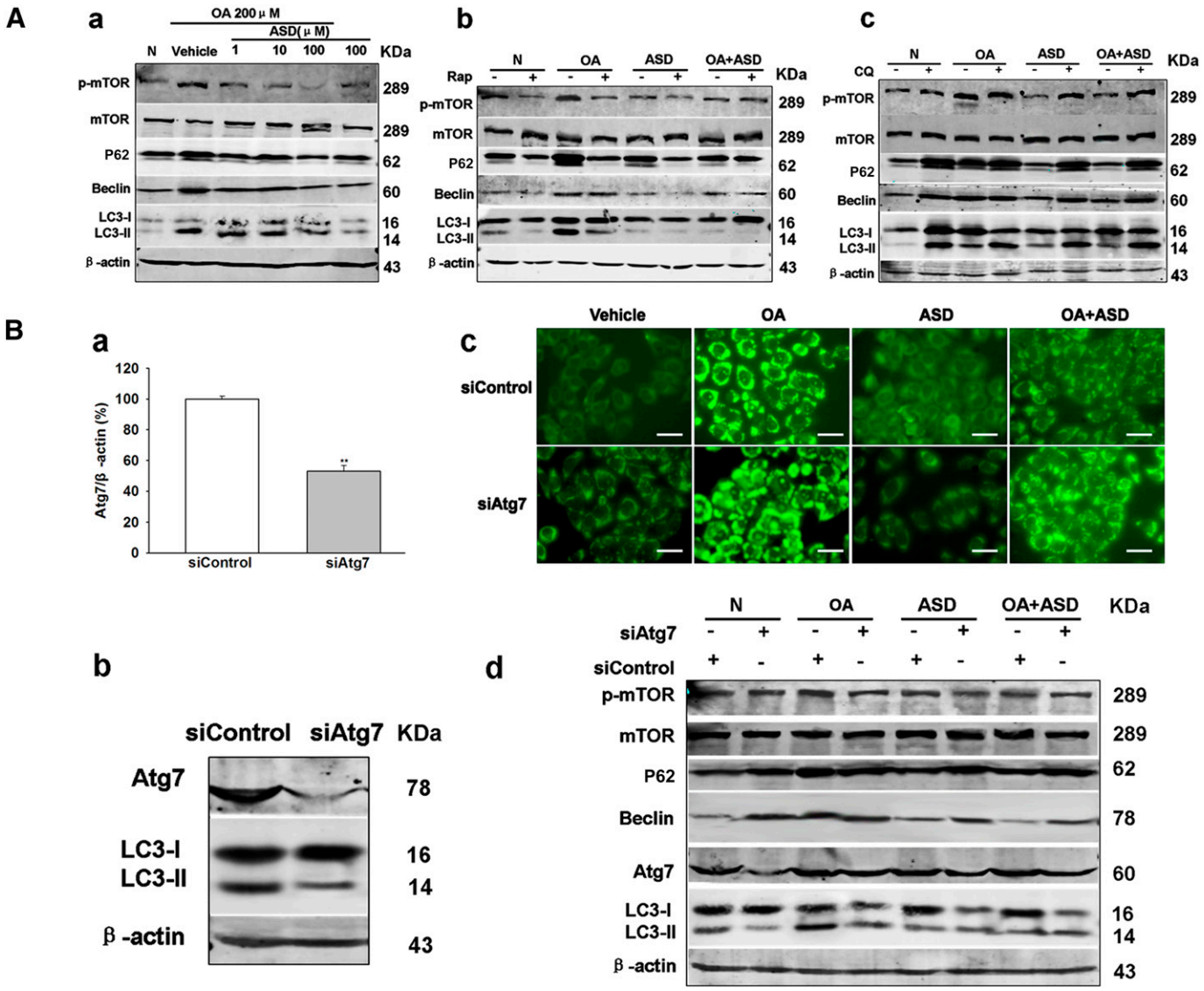

Fig. 6. Effect of ASD on autophagy-related proteins in OA-induced lipid accumulation in BRL cells. (Aa) Total protein was isolated from BRL cells when treated with ASD (1, 10, and 100 μM) and immunoblotted with antibodies for phospho-mTOR, P62, Beclin, LC3, and β-actin. (Ab) Immunoblots of proteins isolated from BRL cells treated with rapamycin (25 ng/ml) and/or ASD (100 μM) and probed with the antibodies shown. (Ac) Immunoblots were conducted in BRL cells treated with CQ (50 nM) and/or ASD (100 μM). Effect of ASD on lipid accumulation when autophagy inhibited. (Ba) Quantification of atg7 after transfection with control or atg7 siRNA. (Bb) Western blots of lysates from BRL cells knocked down with atg7 siRNA. (Bc) Bodipy 493/503 staining of OA- and ASD-treated BRL cells after transfection with control or atg7 siRNA. (Bd) Immunoblots of proteins isolated from siRNA control and siAtg7 cells and probed with the antibodies shown. All values are means ± S.E.M. from three or more independent studies. *$P < 0.05$; **$P < 0.01$. siControl, siRNA control; Scale bar, 200 μm.

BRL cells were infected with siRNAs targeting autophagy gene atg7 or with a control siRNA. Atg7 levels were markedly decreased on immunoblots in siAtg7 cells in parallel with reduced levels of LC3-II, which is compatible with a decrease of autophagic function (Fig. 6B). The effect of ASD on cell lipid droplets was measured in the presence of siAtg7. Knockdown of atg7 abolished the protective effect of ASD. Lipid droplets also significantly increased in the presence of siAtg7 when treated with OA and ASD (Fig. 6Bc). LC3-II levels decreased markedly in siAtg7 cells but not in control siRNA cells and OA- and ASD-treated cells. The levels of LC3-II decreased because interference of autophagy gene atg7 inhibited autophagosome formation. ASD treatment could not prevent OA-induced P62, Beclin, and phospho-mTOR expression.

Discussion

The pathogenesis of NAFLD is not yet fully understood, but studies on lipid accumulation in ob/ob mice and OA-induced BRL cells provide good insight into this pathology. In this study, we found that ASD exerted a strong hepatoprotective effect against NAFLD, and autophagy may contribute to this effect. Autophagy was recently reported to play an important role in hepatic steatosis (Amir and Czaja, 2011; Gracia-Sancho et al., 2014; Kwanten et al., 2014; Lavallard and Gual, 2014). Enhancing autophagy by overexpressing autophagy gene atg7 could improve hepatic steatosis in ob/ob mice and in HFD-fed mice (Yang et al., 2010). Similar results were also observed in the HFD-induced nonalcoholic fatty liver condition when treatment with mTOR inhibitor rapamycin was administered (Lin et al., 2013).

We found that ASD treatment could significantly reduce liver weight, hepatic steatosis, hepatic TG levels, and TC and FFA levels. ASD treatment showed reduced the broken and shrunken of hepatocyte nucleoli. We also demonstrated that ASD treatment attenuated the degree of apoptosis, increased AST and ALT levels and SOD and GSH-PX activity, and decreased MDA. These results suggest that ASD exerted a protective effect against NAFLD. ASD-treated mice had decreased body weight, fat pad weight, and HOMA-IR values. NAFLD is the hepatic manifestation of the metabolic syndrome. As such, it is possible that ASD may have positive effects on systemic components of the disease.

HFD-fed ob/ob mice showed impairment in hepatic autophagic function. The protein amount of P62 was accumulated within the liver of ob/ob mice in parallel with an increase in LC3-II, which indicates that autophagic function was diminished in the liver of ob/ob mice. ASD treatment decreased expression of LC3-II and P62. The level of autophagosomes also significantly increased in the livers of ASD-treated mice. Previous studies showed that an accumulation of P62 reflects a decrease in autophagic flux; on the contrary, activation of autophagic flux leads to a decline in P62 expression (Bjørkøy et al., 2005; Klionsky et al., 2012). The accumulation of LC3-II and autophagosomes may be interpreted as induction of autophagy or a consequence of a blockade of autophagic flux (González-Rodríguez et al., 2014). Therefore, it is conceivable that the decreased expression of LC3-II and P62 observed in ASD-treated mice may reflect activation of autophagic flux.

We performed studies on BRL cells to further confirm the roles of ASD in the reduction of hepatic steatosis and activation of autophagic flux. OA-induced lipotoxicity has a critical role in the pathogenesis of NAFLD. With administration of ASD, a decrease in lipid droplets was observed. EGFP-LC3 fluorescence studies are convenient methods to detect autophagy. ASD significantly enhanced EGFP-LC3 puncta, indicating that ASD increased cell autophagy. The mTagRFP-mWasabi-LC3 reporter was then used to detect the accumulation of autophagosomes and autolysosomes and to monitor autophagic flux. Autophagic flux increased when both yellow and red puncta were increased in cells, whereas autophagic flux was blocked when only yellow puncta were increased without an accompanying increase of red puncta in cells. We found that more autolysosomes were increased than autophagosomes among ASD-treated mice, indicating that autophagic flux was increased.

OA treatment of BRL cells resulted in an accumulation of P62 in parallel with an increase in LC3-II, reflecting a loss of autophagic flux. ASD prevented OA-induced expression of LC3-II, P62, Beclin, and phospho-mTOR. Activation of the autophagy machinery of ASD was demonstrated on several levels, including an examination of LC3-II, P62, Beclin, and phospho-mTOR expression in the absence or presence of rapamycin or CQ. We found that ASD could attenuate autophagic flux blocked by OA, reflecting by reduced phosphorylation of mTOR and decreased P62, LC3-II expression which similar to the effect of rapamycin. Regarding autophagy-induced clearance of hepatic lipid droplets, ASD was no longer able to alleviate lipid accumulation in the presence of siRNA-mediated knockdown of atg7. Moreover, atg7 depletion or CQ treatment abolished the protective effect of ASD which could not decrease LC-II and P62 levels. These data suggested that autophagic flux played a critical role in ASD decreased lipid droplets.

How does ASD increase autophagic flux? Several mechanisms may lead to increased autophagic flux, including 1) promotion of the upstream induction of autophagy and autophagosome biogenesis or 2) increased autophagosomal-lysosomal fusion (Manley et al., 2014). We found that ASD treatment decreased LC3-II and P62 levels; therefore, it is less likely that ASD promotes upstream autophagosome biogenesis. It is likely that ASD might improve autophagic flux by increasing autophagosomal-lysosomal fusion. Indeed, we found that ASD increased not only the EGFP-LC3 puncta but also the yellow and red puncta in the tandem mTagRFP-mWasabi-LC3 assay, which could eventually lead to increased autophagosomal-lysosomal fusion.

In conclusion, our results indicate that ASD mediated alleviation of increased hepatic steatosis targeted at the fusion of autophagosomes to lysosomes. Activation of autophagy in hepatocytes could constitute a therapeutic approach against hepatic steatosis. These results strongly suggest that autophagy modulation via ASD may offer a new strategy for treating NAFLD.

Acknowledgments

The authors thank Dr. Jian Lin for providing the EGFP-LC3, mTagRFP-mWasabi-LC3, and mTagRFP-mWasabi-LC3ΔG plasmids.

Authorship Contributions

Participated in research design: Gong, L. Liu.
Conducted experiments: Gong, Li, Zhang.
Contributed new reagents or analytic tools: H. Liu, Shi.
Performed data analysis: Lv, Han, Wan.
Wrote or contributed to the writing of the manuscript: Gong, Li.

References

Amir M and Czaja MJ (2011) Autophagy in nonalcoholic steatohepatitis. *Expert Rev Gastroenterol Hepatol* **5**:159–166.
Bjørkøy G, Lamark T, Brech A, Outzen H, Perander M, Overvatn A, Stenmark H, and Johansen T (2005) p62/SQSTM1 forms protein aggregates degraded by autophagy and has a protective effect on huntingtin-induced cell death. *J Cell Biol* **171**: 603–614.
Czaja MJ (2010) Autophagy in health and disease. 2. Regulation of lipid metabolism and storage by autophagy: pathophysiological implications. *Am J Physiol Cell Physiol* **298**:C973–C978.
Gong LL, Wang ZH, Li GR, and Liu LH (2014) Protective effects of Akebia saponin D against rotenone-induced hepatic mitochondria dysfunction. *J Pharmacol Sci* **126**: 243–252.
González-Rodríguez A, Mayoral R, Agra N, Valdecantos MP, Pardo V, Miquilena-Colina ME, Vargas-Castrillón J, Lo Iacono O, Corazzari M, Fimia GM, et al. (2014) Impaired autophagic flux is associated with increased endoplasmic reticulum stress during the development of NAFLD. *Cell Death Dis* **5**:e1179.
Gracia-Sancho J, Guixé-Muntet S, Hide D, and Bosch J (2014) Modulation of autophagy for the treatment of liver diseases. *Expert Opin Investig Drugs* **23**:965–977.
Jeong SI, Zhou B, Bae JB, Kim NS, Kim SG, Kwon J, Kim DK, Shin TY, Jeon H, Lim JP, et al. (2008) Apoptosis-inducing effect of Akebia saponin D from the roots of Dipsacus asper Wall in U937 cells. *Arch Pharm Res* **31**:1399–1404.
Klionsky DJ, Abdalla FC, Abeliovich H, Abraham RT, Acevedo-Arozena A, Adeli K, Agholme L, Agnello M, Agostinis P, Aguirre-Ghiso JA, et al. (2012) Guidelines for the use and interpretation of assays for monitoring autophagy. *Autophagy* **8**: 445–544.
Kwanten WJ, Martinet W, Michielsen PP, and Francque SM (2014) Role of autophagy in the pathophysiology of nonalcoholic fatty liver disease: a controversial issue. *World J Gastroenterol* **20**:7325–7338.
Lan Y, Lei N, Zhang XF, Yang R, Li C, and Liu L (2011) Hypolipidemic function with liver protection of extracts from Dipsacus asper on nonalcoholic fatty liver disease in mice and its active fractions. *Chin Tradit Herbal Drugs* **42**:2497–2501.
Lavallard VJ and Gual P (2014) Autophagy and non-alcoholic fatty liver disease. *BioMed Res Int* **2014**:120179.
Lazo M and Clark JM (2008) The epidemiology of nonalcoholic fatty liver disease: a global perspective. *Seminars in liver disease* **28**:339–350.
Li C, Gao Y, Tian J, Xing Y, Zhu H, and Shen J (2012) Long-term oral Asperosaponin VI attenuates cardiac dysfunction, myocardial fibrosis in a rat model of chronic myocardial infarction. *Food Chem Toxicol* **50**:1432–1438.
Li C, Liu Z, Tian J, Li G, Jiang W, Zhang G, Chen F, Lin P, and Ye Z (2010a) Protective roles of Asperosaponin VI, a triterpene saponin isolated from Dipsacus asper Wall on acute myocardial infarction in rats. *Eur J Pharmacol* **627**:235–241.
Li C, Tian J, Li G, Jiang W, Xing Y, Hou J, Zhu H, Xu H, Zhang G, Liu Z, et al. (2010b) Asperosaponin VI protects cardiac myocytes from hypoxia-induced

apoptosis via activation of the PI3K/Akt and CREB pathways. *Eur J Pharmacol* **649**:100–107.
Li C, Zhang XF, Ya-Li Lv, Lan YY, Ning L, and Liu L (2012) Hepatoprotective effect of Akebia saponin D on the acute liver injury induced by CCl4 in mice. *West Chin J Pharm Sci* **27**:257–259.
Lin CW, Zhang H, Li M, Xiong X, Chen X, Chen X, Dong XC, and Yin XM (2013) Pharmacological promotion of autophagy alleviates steatosis and injury in alcoholic and non-alcoholic fatty liver conditions in mice. *J Hepatol* **58**:993–999.
Manley S, Ni HM, Kong B, Apte U, Guo G, and Ding WX (2014) Suppression of autophagic flux by bile acids in hepatocytes. *Toxicol Sci* **137**:478–490.
Matteoni CA, Younossi ZM, Gramlich T, Boparai N, Liu YC, and McCullough AJ (1999) Nonalcoholic fatty liver disease: a spectrum of clinical and pathological severity. *Gastroenterology* **116**:1413–1419.
Niu Y, Li Y, Huang H, Kong X, Zhang R, Liu L, Sun Y, Wang T, and Mei Q (2011) Asperosaponin VI, a saponin component from Dipsacus asper wall, induces osteoblast differentiation through bone morphogenetic protein-2/p38 and extracellular signal-regulated kinase 1/2 pathway. *Phytother Res* **25**:1700–1706.
Peng LH, Ko CH, Siu SW, Koon CM, Yue GL, Cheng WH, Lau TW, Han QB, Ng KM, Fung KP, et al. (2010) In vitro & in vivo assessment of a herbal formula used topically for bone fracture treatment. *J Ethnopharmacol* **131**:282–289.
Singh R, Kaushik S, Wang Y, Xiang Y, Novak I, Komatsu M, Tanaka K, Cuervo AM, and Czaja MJ (2009) Autophagy regulates lipid metabolism. *Nature* **458**:1131–1135.
Smith BW and Adams LA (2011) Non-alcoholic fatty liver disease. *Crit Rev Clin Lab Sci* **48**:97–113.
Yang L, Li P, Fu S, Calay ES, and Hotamisligil GS (2010) Defective hepatic autophagy in obesity promotes ER stress and causes insulin resistance. *Cell Metab* **11**: 467–478.
Yu X, Wang LN, Ma L, You R, Cui R, Ji D, Wu Y, Zhang CF, Yang ZL, and Ji H (2012) Akebia saponin D attenuates ibotenic acid-induced cognitive deficits and pro-apoptotic response in rats: involvement of MAPK signal pathway. *Pharmacol Biochem Behav* **101**:479–486.
Zhou C, Zhong W, Zhou J, Sheng F, Fang Z, Wei Y, Chen Y, Deng X, Xia B, and Lin J (2012) Monitoring autophagic flux by an improved tandem fluorescent-tagged LC3 (mTagRFP-mWasabi-LC3) reveals that high-dose rapamycin impairs autophagic flux in cancer cells. *Autophagy* **8**:1215–1226.
Zhou YQ, Yang ZL, Xu L, Li P, and Hu YZ (2009) Akebia saponin D, a saponin component from Dipsacus asper Wall, protects PC 12 cells against amyloid-beta induced cytotoxicity. *Cell Biol Int* **33**:1102–1110.

Address correspondence to: Li-hong Liu, Beijing Chao-Yang Hospital, Capital Medical University, 8 Gongren Tiyuchang Nanlu, Beijing 100020, China. E-mail: hongllh@126.com